Check for updates

Fitting analysis of the curve of main inclined section of surface subsidence of insufficient mining

Wei Du[1], Ming Guo[2], Jia Lai[2], Yang Zhang[2], Yafei Ma[3]*,
Huoda Dun[3], Boyuan Jia[3], Libiao Feng[3] and Zhiqiang Li[4]

[1]Shanxi Xiaobaodang Mining Co.,Ltd., Yulin, Shaanxi, China, [2]Shanxi Coalbed Methane Development
Co.,Ltd., Xianyang, Shaanxi, China, [3]College of Urban Geology and Engineering, Hebei GEO University
Shijiazhuang, Shijiazhuang, Hebei, China, [4]Hebei Civil Engineering Co., Ltd., Shijiazhuang, Hebei, China

Based on the measured subsidence data of the 112,201 working face in Xiaobaodang Coal Mine of Shaanxi Province, the traditional probability integral method and probability density function method are used to study the curve fitting of the main inclined section under insufficient mining conditions. The analysis results show that the fitting effect of the probability density function method is better than that of the probability integral method. In view of the poor effect of edge fitting, the idea of sub-region fitting is proposed. Two sets of predicted parameters are used to fit the edge and central regions. The fitting results are close to the surface deformation, and the fitting effect is better. The method can improve the accuracy of surface deformation prediction. The research results can provide a reference for the prediction of surface subsidence in Xiaobaodang Coal Mine and its surrounding mining areas.

1 Introduction

After mining an underground coal seam, the original stress equilibrium of the surrounding rock mass is disrupted, leading to stress redistribution until a new equilibrium is reached. During this process, the rock strata and ground surface undergo continuous movement, deformation, and discontinuous damage, a phenomenon known as mining subsidence. Mining subsidence is a significant geological hazard in mining areas. Currently, the probabilistic integration method (PIM), developed by Liu Baochen and Dai Huayang based on the random media theory (Liu and Dai, 2016). is the dominant approach for predicting coal mining subsidence. The PIM calculates subsidence via error functions and exhibits high practicality due to its simple parameterization. However, under insufficient mining conditions—where the mining range does not reach the critical threshold for full subsidence development—its limitations become evident, necessitating further improvements. Such as Cai et al. (2023), provide a comprehensive analysis of monitoring and calculation methods, emphasizing the method's foundation in random media theory and its limitations under varying geological conditions. The probabilistic integration method has certain limitations, including its inability to accurately represent rock mass movement and deformation within the strata (Chen et al., 2021), rapid edge convergence, and insufficient explanation of the underlying mechanical mechanisms. Among the many models, the probability density function method proposed by Guo Zengzhang has achieved good fitting effects (Guo et al., 2004). Yan et al. (2019) studied the problem of ground subsidence

caused by coal mining and proposed a new prediction model based on the log-normal distribution function. Zhang et al. (2020) proposed an improved Knothe time function model for predicting dynamic ground subsidence caused by underground mining. Wang and Yang (2021) investigated the relationship between the parameters of the Gompertz time function and geological mining conditions, and proposed a calculation method and prediction algorithm for practical application. Hu et al. (2023) combined InSAR technology, the probabilistic integration method, and the genetic algorithm to propose an improved method for dynamically predicting the probabilistic integration parameters for achieving subsidence inversion and prediction under insufficient mining conditions. Zi-Tong et al. (2024) proposed a system framework (BASIC-H) based on Bayesian inference and Copula theory, for modeling and constructing the probability density function (PDF) and credible region (CR) of multivariate, asymmetric, and multimodal distributions of geological technical data. Shi et al. (2021) integrated SBAS-InSAR with the probability integral method (PIM) to improve subsidence prediction accuracy. Wang et al. (2024) proposed an improved dynamic PIM combined with InSAR, effectively reducing edge effects in subsidence predictions. Li et al. (2022) introduced a strip-unit mining model based on the PIM to achieve accurate 3D dynamic subsidence predictions. Chi et al. (2023) developed a hybrid machine-learning model that improved the accuracy of predicting PIM parameters. Guo et al. (2022) introduced an improved fireworks algorithm to enhance the reliability of PIM parameter inversion. Lou, (2024) applied robust ridge regression to achieve more stable and accurate PIM parameter estimation, overcoming issues related to outliers and ill-conditioned matrices. These advancements demonstrate the international relevance and continuous improvement in subsidence prediction methodologies. Tao et al. (2023), in response to the actual range of surface impact from coal seam mining in thick loose layer mining areas significantly exceeding theoretical predictions, proposed a new segmented correction model of the probabilistic integration method. Zhang et al. (2024) studied the surface subsidence prediction of the Gengquan coal mine based on the probabilistic integration method and the FLAC3D numerical simulation method. Xuemin et al. (2021) proposed a new dynamic prediction integrated model (DPIM), based on the integration of the probabilistic integration method (PIM) and the Weibull time function, for predicting future dynamic subsidence during periods not covered by SAR data acquisition. Bing et al. (2021) applied the probability density function method to predict surface subsidence and rock layer conditions in a mining subsidence area. Many scholars have modified and improved the model, achieving certain results (Luo et al., 2024; Huo et al., 2023; Yuan et al., 2020; Li et al., 2020; Zhao et al., 2022; Wei et al., 2023), with specific adaptations for conditions such as reverse faulting (Luo et al., 2024) and backfill mining (Huo et al., 2023), addressing issues such as rapid convergence at the edges. Ground settlement is a common geological hazard associated with underground engineering activities such as mining and tunneling. For instance, Ahmadi et al. (2023) investigated the impact of tunneling on bridge foundations in urban areas, highlighting that excavation-induced ground settlement significantly affects adjacent structures. Similarly, mining activities, particularly under-extraction, can also lead to ground settlement, posing risks to surface structures and ecosystems.

At present, one of the widely adopted methods is to conduct subsidence observation through surface observation stations, and to predict the subsidence of other areas by using the actual measurement data to invert for prediction parameters (Guo et al., 2004). This requires the selected model to have a good fit, so it is of great significance to study the fitting accuracy of the subsidence function curve.

This study utilizes actual subsidence measurements to evaluate the curve-fitting performance of the traditional probabilistic integration method and the probability density function method for the main inclined cross-section under insufficient mining conditions. Under insufficient mining conditions, there is a significant discrepancy between the predicted results and the actual situation (Zhao et al., 2022; Wei et al., 2023; Jiang et al., 2024), prompting studies like Yuan et al. (2020) to focus on parameter reliability.

These recent advancements, including modifications for thick loose layers (Li et al., 2020; Zhao et al., 2022) and loess dongas (Wei et al., 2023), underscore the ongoing efforts to refine subsidence prediction models for complex mining scenarios.

In this study, multiple approaches were explored to optimize data fitting. Initially, cumulative distribution function (CDF) and probability density function (PDF) methods were employed to model the marginal distribution of the data. However, these standard techniques failed to capture key data characteristics. However, these standard techniques did not adequately capture the characteristics of the data. To address this issue, we introduced a piecewise fitting strategy, which involved modeling different segments of the data separately. This approach significantly improved the flexibility and accuracy of the fit. Subsequently, we validated our findings through numerical simulations, confirming that the developed model effectively reflects the overall trend of the data.

2 Non-sufficient mining surface movement model

2.1 Probabilistic integration method

Liu Baochen and Dai Huayang developed the probabilistic integration prediction method, deriving a simplified solution based on random media theory and formulating a comprehensive, applicable approach (Liu and Dai, 2016).

(1) The semi-infinite mining prediction formula is as follows:

The insufficient settlement function is given in Equation 1, where the error function (*erf*) describes the integral results of the probability distribution, reflecting the cumulative effects of random medium movement.

$$W(x) = \frac{W_0}{2}\left[erf\left(\frac{\sqrt{\pi}}{r}x\right) + 1 \right] \tag{1}$$

By differentiating Equation 1, the formula for calculating surface inclination (slope) is obtained, as shown in Equation 2.

$$i(x) = \frac{W_0}{r}e^{-\frac{\pi^2}{r^2}} \tag{2}$$

Further differentiation of Equation 2 yields the formula for calculating subsidence curvature along the main section, as shown in Equation 3.

$$K(x) = -\frac{2\pi W_0}{r^3} x e^{-\pi \frac{x^2}{r^2}}$$ (3)

By differentiating Equation 3, the formula for calculating horizontal deformation along the main section is obtained, as shown in Equation 4.

$$U(x) = b W_0 e^{-\pi \frac{x^2}{r^2}}$$ (4)

By taking the derivative of Equation 4, the formula for calculating the horizontal deformation along the main section can be obtained, as shown in Equation 5.

$$\varepsilon(x) = -\frac{2\pi b W_0}{r^2} x e^{-\pi \frac{x^2}{r^2}}$$ (5)

Where, w_0–Maximum surface subsidence, mm; r–Influence radius, m; x–Horizontal position of any point; b–Horizontal movement coefficient.

(2) Prediction of Surface Movement and Deformation on the Main Inclined Cross-Section

When the coal seam is fully mined along the strike direction (parallel to the coal seam extension) with a sufficiently large mining range and complete surface subsidence, but mining in the dip direction (perpendicular to the strike) remains limited, the subsidence basin becomes asymmetric. To account for this asymmetry, the probabilistic integration method must be modified by introducing the main influence radii (r_1 and r_2) in the lower and upper mountain directions. These parameters correspond to the influence range beneath the coal seam (lower mountain) and above the coal seam (upper mountain), respectively.

The modified prediction formulas for the dip-direction main cross-section are presented in Equations 6–10:

$$W^0(y) = W(y, t_1) - W(y - L, t_2)$$ (6)

$$i^0(y) = i(y, t_1) - i(y - L, t_2)$$ (7)

$$K^0(y) = K(y, t_1) - K(y - L, t_2)$$ (8)

$$U^0(y) = U(y, t_1) - U(y - L, t_2)$$ (9)

$$\varepsilon^0(y) = \varepsilon(y, t_1) - \varepsilon(y - L, t_2)$$ (10)

In the formula, t_1 and t_2 represent parameters for the lower and upper mountain boundaries, respectively. The main influence radii of the equivalent horizontal coal seam in these two directions are no longer identical. The radii r_1 and r_2, can be determined using Equation 11:

$$r_1 = \frac{H_2}{tan\beta_1}, \qquad r_2 = \frac{H_2}{tan\beta_2}$$ (11)

Here, $tan\beta_1$ and $tan\beta_2$ represent the tangents of the main influence angles for the lower and upper mountain regions, respectively. The inclined working face length L is calculated using Equation 12:

$$L = (D_1 - s_1 - s_2)\frac{sin(\theta_0 + \alpha)}{sin\theta_0}$$ (12)

where D_1 is the working face length, θ_0 is the mining influence propagation angle, and α is the coal seam inclination angle.

The above formula applies to limited mining and does not differentiate between sufficient and insufficient mining conditions. Typically, insufficient mining values are obtained by multiplying the sufficient mining values by a mining coefficient C, as expressed in Equation 13:

$$W_0(y) = C\frac{W_0}{2}\left\{ \left[erf\left(\frac{\sqrt{\pi}}{r}x\right) + 1 \right] - \left[erf\left(\frac{\sqrt{\pi}}{r}x - D_1 + s_1 + s_2\right) + 1 \right] \right\}$$ (13)

In the probabilistic integration method, subsidence basin parameters are typically solved using mathematical techniques, with curve fitting based on actual measurement data being the most common approach. The mathematical solution process involves identifying a smooth curve that minimizes the sum of squared errors of discrete data points. The predicted parameters include the subsidence coefficient q, the tangent of the main influence angle $tan\beta$, the mining influence propagation coefficient K, the horizontal movement coefficient b, and the inflection point offset distance S, etc.

The primary challenges in parameter estimation are as follows:

(1) High correlation between parameters: When multiple parameters exhibit strong correlation, they become indistinguishable during curve fitting. For instance, the mining coefficient C and the subsidence coefficient q are difficult to separate. In the formula $Cw_0/2$, the expression transforms into $Cmqcos\alpha/2$, meaning that during fitting, it effectively scales mmm by a factor of C and q, making it difficult to distinguish between C and q.
(2) Poor fitting at basin edges: Ensuring accurate fitting across both the interior and edge regions of the subsidence basin is challenging. While the central part of the basin can typically be well-fitted, the edge regions often exhibit rapid convergence, leading to poor fitting performance (Han, 2021).

2.2 Probability density function method

The probability density function (PDF) method postulates that under conditions of insufficient mining, the displacement probability of discrete medium fragments gradually converges to the probability density function of a normal distribution (Guo et al., 2004). Assuming that the movement of fractured rock mass units follows a normal distribution, the subsidence model can be directly constructed using the probability density function, effectively mitigating strong correlations between parameters. The specific subsidence formula based on the probability density function method is presented in Equation 14:

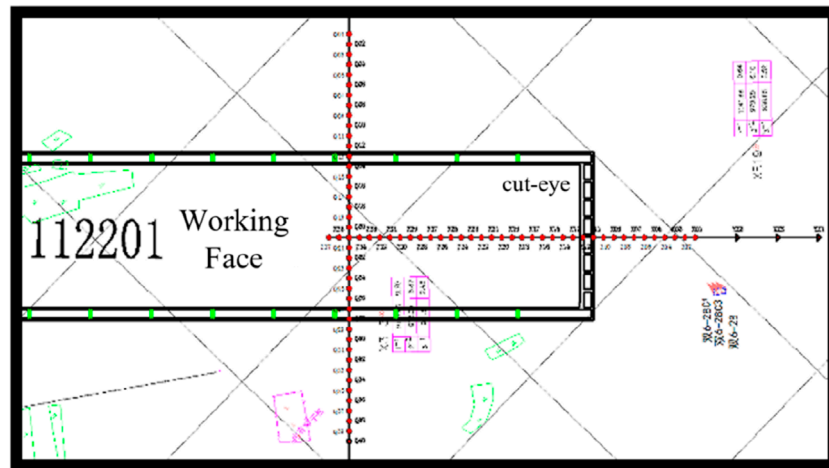$$w(x) = w_{max} exp\left[-\pi\frac{(x - L_1)^2}{r^2} \right]$$ (14)

FIGURE 1
Schematic of monitoring points on strike and dip observation lines.
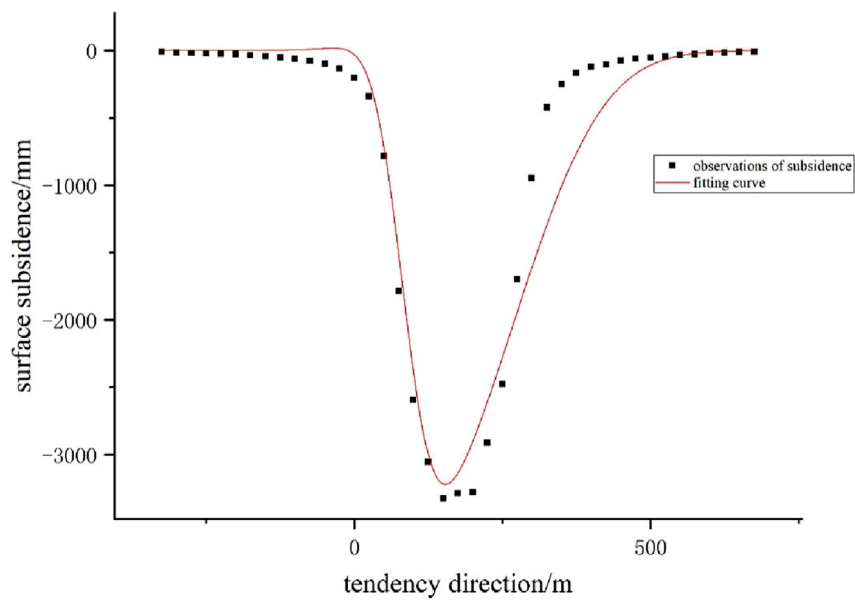

FIGURE 2
Fitting curve of the ground subsidence probability integration method for the 112,201 working face.

$$i(x) = -2\pi w_{max} \frac{x - L_1}{r^2} exp\left[-\pi \frac{(x - L_1)^2}{r^2}\right] \qquad (15)$$

$$k(x) = \frac{2\pi w_{max}}{r^2}\left[\frac{2\pi(x - L_1)^2}{r^2} - 1\right] exp\left[-\pi \frac{(x - L_1)^2}{r^2}\right] \qquad (16)$$

$$U(x) = 2\pi b w_{max} \frac{x - L_1}{r} exp\left[-\pi \frac{(x - L_1)^2}{r^2}\right] \qquad (17)$$

$$\varepsilon(x) = \frac{2\pi w_{max}}{r^2}\left[\frac{2\pi(x - L_1)^2}{r^2} - 1\right] exp\left[-\pi \frac{(x - L_1)^2}{r^2}\right] \qquad (18)$$

Equations 15–18 provide the calculation formulas for surface inclination, curvature, horizontal displacement, and horizontal deformation under the probability density function (PDF) method. These equations follow a similar structure to Equations 2–5.

In the formula: w_{max} represents the maximum surface subsidence under insufficient mining conditions, given by $w_{max} = mq cos$, where m is the coal seam thickness, q is the subsidence rate, and α is the coal seam inclination angle; x is the horizontal distance from a point within the main cross-section to the center of the mined-out area; r is the main influence radius, expressed as $r = H/tan\beta$, where H is the mining depth and β is the main influence angle. b is the horizontal movement coefficient. L is the working face length, where $L_1 = 1/2$.

TABLE 1 Table of fitting residual values for the probability integration method of the 112,201 working face.

Monitoring point	Fitted residual value/mm	Observed value/mm	Monitoring point	Fitted residual value/mm	Observed value/mm
Q01	−9.00	−9	Q21	−376.42	−3,278
Q02	−18.01	−18	Q22	−308.65	−2,913
Q03	−20.01	−20	Q23	−201.78	−2,480
Q04	−22.04	−22	Q24	244.32	−1,697
Q05	−27.09	−27	Q25	660.58	−948
Q06	−29.21	−29	Q26	868.82	−425
Q07	−37.49	−37	Q27	755.57	−253
Q08	−45.08	−44	Q28	591.92	−169
Q09	−55.28	−53	Q29	431.94	−123
Q10	−68.63	−64	Q30	282.82	−108
Q11	−86.89	−78	Q31	188.54	−77
Q12	−114.89	−100	Q32	111.92	−62
Q13	−147.54	−133	Q33	55.74	−54
Q14	−172.07	−204	Q34	21.67	−45
Q15	−114.20	−344	Q35	4.97	−34
Q16	−63.95	−785	Q36	−6.09	−28
Q17	−262.92	−1785	Q37	−7.16	−19
Q18	−199.88	−2,593	Q38	−11.85	−18
Q19	−53.81	−3,056	Q39	−7.93	−11
Q20	−110.25	−3,327	Q40	−7.53	−9

Analysis of the fitting results and corresponding data indicates a goodness-of-fit of 0.93, with relatively large fitting errors at the edges.

Compared to the probabilistic integration method, the PDF method directly uses the subsidence rate to predict maximum subsidence under insufficient mining conditions. This approach eliminates the need for two additional parameters—the mining coefficient and the subsidence coefficient—simplifying the prediction process.

3 Working face and surface movement conditions

3.1 Overview of the working face

The Xiao Ba Dang coal mine, operated by Xiao Ba Dang Mining Co., Ltd., is located in southwest Shenmu County, Yulin City, Shaanxi Province, and northeast Yuyang District. The first mining working face, 112,201, employs the large mining height longwall top coal caving method for roof management. After mining, the roof

collapses and fractures, forming an "internal three zones" within the rock strata.

The 112,201 working face has a strike length of 4,660 m and a dip length of 350 m. The coal seam thickness ranges from 5.5 to 6.0 m, with an average of 5.8 m, and an inclination angle averaging 0.5°.

3.2 Overview of the observation station

The surface topography of the 112,201 working face is relatively simple, with no buildings, railways, pipelines, or other obstructions. Consequently, the observation station in this study adopts a linear layout consisting of a strike observation line and a dip observation line, both perpendicular at the center of the subsidence basin.

Design of the strike observation line:

Given the thick surface loose layer of the 112,201 working face, the strike observation line is designed to cover half of the subsidence basin. Based on surface movement observations from the 20,102
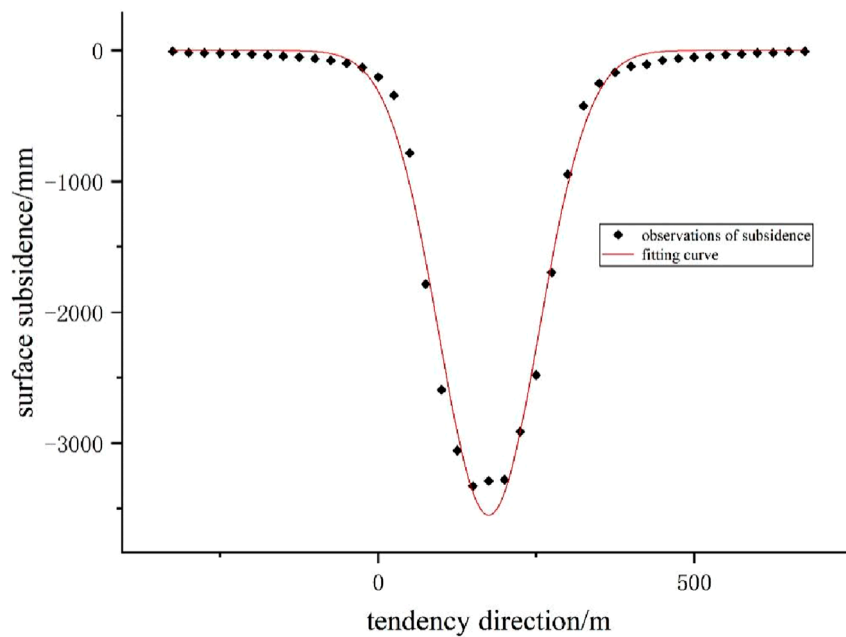
FIGURE 3
Fitting curve graph of the ground subsidence using the probability density function method for the 112,201 working face.

working face of the Yushuwan coal mine, the strike line length is set at 900 m, with 300 m extending beyond the mining boundary of the cut eye and 600 m within it.

At one end of the strike line, three control points are placed outside the cut eye, spaced 100 m apart. Considering the average mining depth of 302 m, the point spacing is 25 m, resulting in a total of 37 monitoring points along the strike line. The monitoring point numbering follows a sequential pattern: Control points are labeled KZ01, KZ02, KZ03. Monitoring points are identified using a character and two Arabic numerals (e.g., Z01, Z02, …). "K" denotes a control point. "Z" denotes the strike observation line. The following numbers represent the sequential measuring points.

Design of the dip observation line:

To ensure complete subsidence basin coverage, the dip observation line length is set at 1,000 m, meeting observation requirements.

Each end of the dip line has two control points, totaling four, with a spacing of 100 m between control points and working points. Since the working face width (l = 350 m) is less than (1.4 H$_0$ = 423 m), the movement basin may not have reached full mining conditions along the dip. To accurately determine point spacing, 25 m intervals are used, with 40 working measuring points laid out. The order of the dip observation line control points is KQ01, KQ02, KQ04; the working measuring point number is composed of a character and two Arabic numerals. For example, the first monitoring point on the dip observation line is numbered as Q01, and the rest follow suit. Where "K" is the control point identification code, "Q" is the monitoring point identification code, and the following numbers are the sequential numbers of the measuring points.

The layout of strike and dip observation line monitoring points is illustrated in Figure 1.

3.3 Observation data analysis

The working face is fully mined along the strike direction, with a maximum settlement of 3,664 mm recorded at monitoring point Z18. In the dip direction, the maximum settlement reaches 3,327 mm at point Q20, and the settlement curve does not exhibit a horizontal section. A comprehensive analysis indicates that full mining conditions have not been achieved in the dip direction.

4 Surface subsidence trend main cross-section fitting analysis

The fitting analysis in this study was conducted using Origin, a professional plotting and data analysis software developed by OriginLab Corporation. Widely used internationally, Origin provides robust function fitting capabilities (Grant, 2017). In this study, Origin was employed for nonlinear fitting of subsidence data. Its built-in algorithms enabled the construction of probability integration and density function models, with residual analysis performed to evaluate goodness-of-fit. Its built-in algorithms facilitated the construction of probability integration and probability density function models, while residual analysis was performed to assess the goodness-of-fit.

4.1 Probabilistic integration method fitting analysis

Using the nonlinear fitting function in Origin, a probabilistic integration fitting function was constructed based on Equation 13. Since the existing surface subsidence data use the left mining

TABLE 2 Table of fitting residual values using the probability density function method for the 112,201 working face.

Monitoring point	Fitted residual value/mm	Observed value/mm	Monitoring point	Fitted residual value/mm	Observed value/mm
Q01	−9.00	−9	Q21	99.17	−3,278
Q02	−18.00	−18	Q22	−2.14	−2,913
Q03	−20.00	−20	Q23	−207.68	−2,480
Q04	−22.00	−22	Q24	−90.45	−1,697
Q05	−26.99	−27	Q25	80.73	−948
Q06	−28.95	−29	Q26	171.60	−425
Q07	−36.78	−37	Q27	60.36	−253
Q08	−43.18	−44	Q28	−19.93	−169
Q09	−50.16	−53	Q29	−58.77	−123
Q10	−55.14	−64	Q30	−82.94	−108
Q11	−52.94	−78	Q31	−68.14	−77
Q12	−35.77	−100	Q32	−59.16	−62
Q13	16.07	−133	Q33	−53.18	−54
Q14	109.36	−204	Q34	−44.78	−45
Q15	252.60	−344	Q35	−33.95	−34
Q16	243.73	−785	Q36	−27.99	−28
Q17	−178.45	−1785	Q37	−19.00	−19
Q18	−320.68	−2,593	Q38	−18.00	−18
Q19	−145.14	−3,056	Q39	−11.00	−11
Q20	50.17	−3,327	Q40	−9.00	−9

Analysis of the fitting results and corresponding data shows a goodness-of-fit of 0.989, indicating a superior fitting performance compared to the probabilistic integration method. However, relatively large fitting errors persist at the edges.

boundary as the origin, the independent variable x in the original formula requires a coordinate translation by s_1. Thus, the original coordinates are replaced with $(x-s_1)$. Incorporating the parameters of the 112,201 working face and surface observation data, the reconstructed probabilistic integration fitting function, which includes the inflection point shift, is presented in Equation 19:

$$W_0(y) = C \frac{5800 \times q}{2} \left\{ \left[erf\left(\frac{\sqrt{\pi} \times tan\beta}{302}(x - s_1) \right) + 1 \right] - \left[erf\left(\frac{\sqrt{\pi} \times tan\beta}{302}(x - 305 + s_2) \right) + 1 \right] \right\} \quad (19)$$

Fitting the model using the aforementioned function reveals a correlation between C and q. Therefore, it is necessary to assign a value to C based on actual conditions. The value of C is determined as the ratio of the maximum subsidence in the dip direction to the

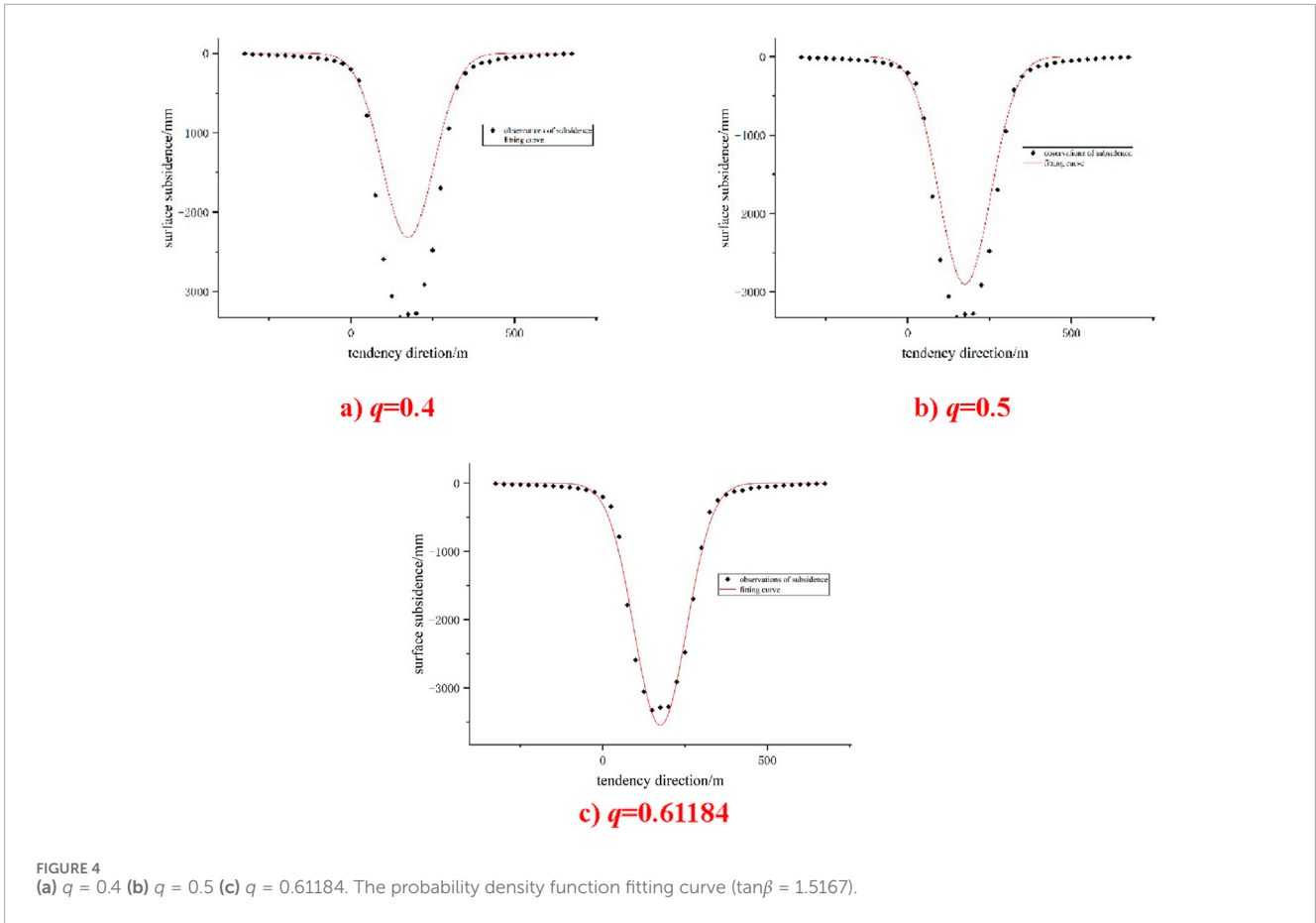maximum subsidence in the strike direction. After calculation, C is found to be 0.9.

Since the coal seam is nearly horizontal, it can be assumed that s_1 and s_2 are equal. Thus, a single variable s is used in the formula instead. The simplified probabilistic integration fitting function is presented in Equation 20:

$$W_0(y) = 2600 \times q \left\{ \left[erf\left(\frac{\sqrt{\pi} \times tan\beta}{302}(x - s) \right) + 1 \right] - \left[erf\left(\frac{\sqrt{\pi} \times tan\beta}{302}(x - 305 + s) \right) + 1 \right] \right\} \quad (20)$$

Among them, q, $tan\beta$ and s are the predicted parameters.

The fitting curve is shown in Figure 2, and the fitting residual results are shown in Table 1:

The fitting parameters of the aforementioned curve are as follows: $q = 1.02$, $tan\beta = 2.97$, and $S = 82.38$.

FIGURE 4
(a) q = 0.4 **(b)** q = 0.5 **(c)** q = 0.61184. The probability density function fitting curve (tanβ = 1.5167).

4.2 Probability density function method

The probability density function (PDF) fitting function, constructed based on Equation 14, is presented in Equation 21:

$$w(x) = -5800 \times q \times \exp\left[-\pi \frac{(x-175)^2 \times tan^2\beta}{302^2}\right] \quad (21)$$

The fitting curve is illustrated in Figure 3, while the fitting residuals are presented in Table 2.

The fitting parameters of the aforementioned curve are as follows: q = 0.61184, tanβ = 1.5167, and S = 82.38.

4.3 Sensitivity analysis of q and $tan\beta$

The sensitivity of q and tan β is now discussed and analyzed.

(1) q

Under the condition that $tan\beta$ remains constant at 1.5167, Figure 4 shows the fitted probability density function curves for different cases where q = 0.4, q = 0.5, and q = 0.61184.

Overall, under the constant condition of $tan\beta$ = 1.5167, an increase in the value of q leads to a reduction in the degree of surface subsidence, while the symmetrical U-shaped distribution characteristic of the subsidence remains unchanged. This trend indicates that q is a critical parameter affecting the depth of

subsidence, with larger q values corresponding to shallower subsidence.

(2) $tan\beta$

Under the condition that q remains constant at 0.61184, Figure 5 shows the fitted probability density function curves for different cases where $tan\beta$ = 1.5167, $tan\beta$ = 2, and $tan\beta$ = 3.

Under the condition that q remains constant at 0.61184, as $tan\beta$ increases from 1.5167 to two and then to 3, the following trends are observed: The maximum depth (peak value) of surface subsidence gradually increases. The range of subsidence distribution gradually narrows, with the curve becoming steeper, indicating that subsidence is more concentrated in the central region. The overall distribution retains a symmetrical U-shaped characteristic, with the basic shape unchanged by variations in $tan\beta$.

By adjusting the expected parameters in the fitting of the predicted curve to the observation data, it is difficult to ensure that both the interior and the edges of the basin can be well fitted.

When q remains constant at 0.61184, and $tan\beta$ increases from 1.5167 to 2, and then to 3, the following trends are observed:

1. The maximum depth (peak value) of surface subsidence gradually increases.
2. The subsidence distribution range narrows, with the curve becoming steeper, indicating that subsidence is more concentrated in the central region.
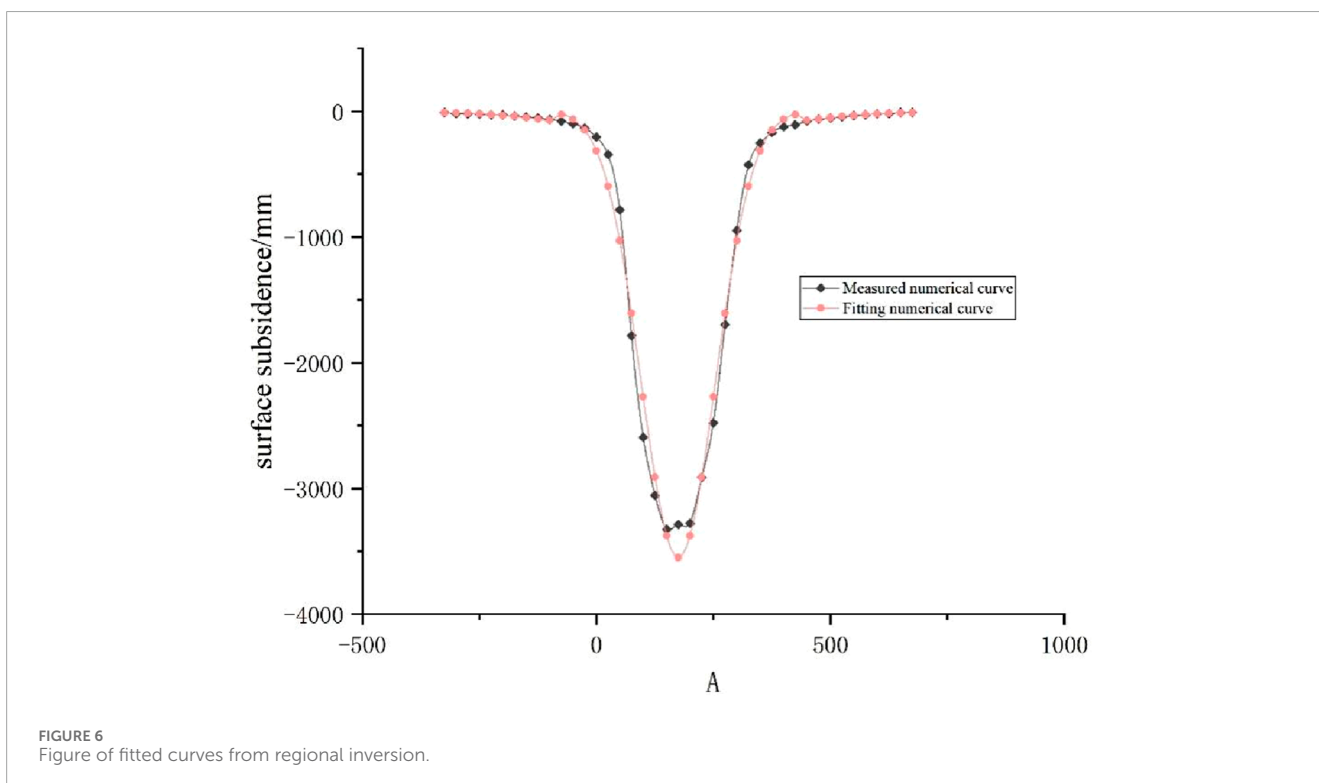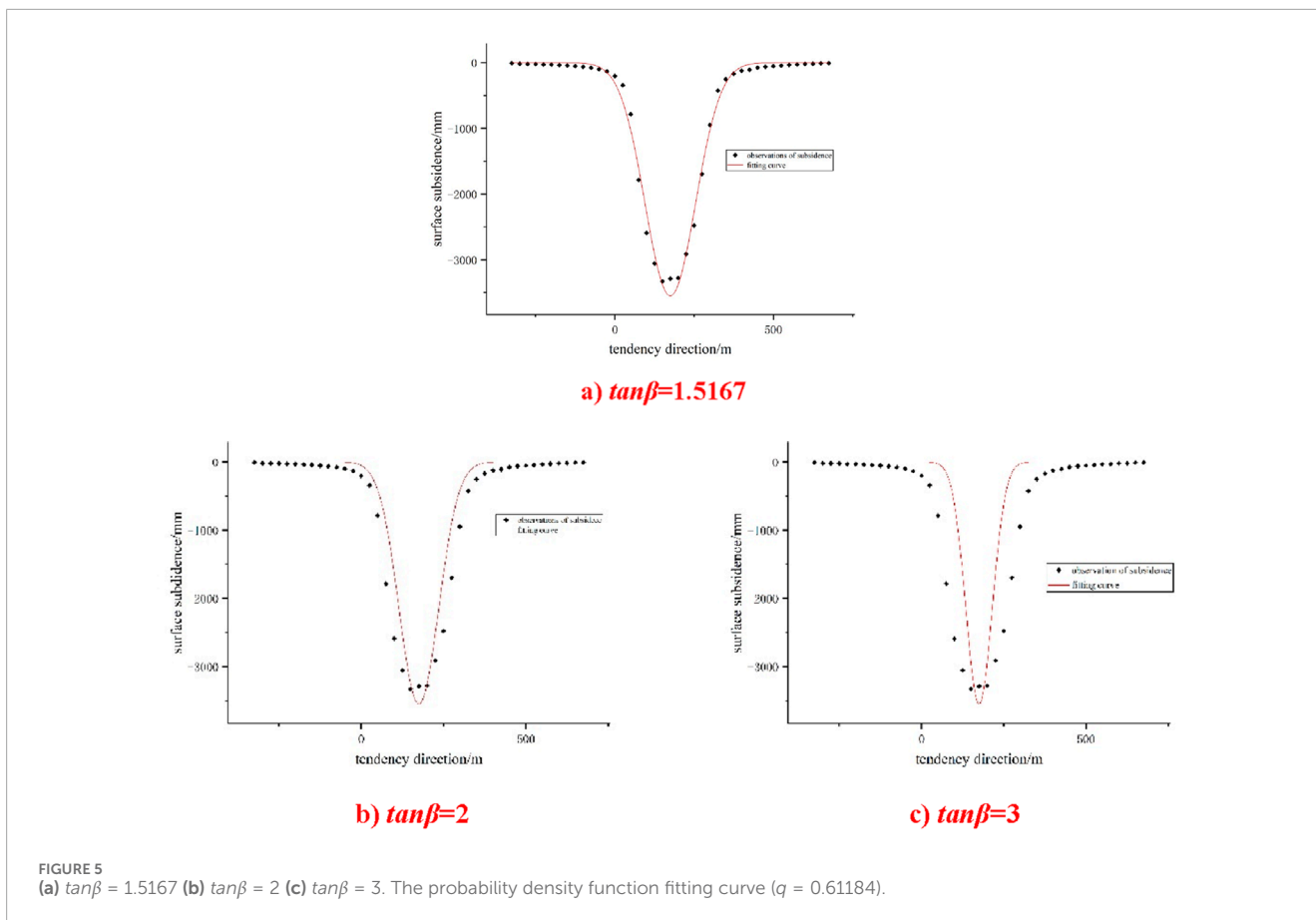
FIGURE 5
(a) *tanβ* = 1.5167 **(b)** *tanβ* = 2 **(c)** *tanβ* = 3. The probability density function fitting curve (*q* = 0.61184).

FIGURE 6
Figure of fitted curves from regional inversion.

TABLE 3 Table of fitting residual values for edge data using the probability density function method for the 112,201 working face.

Monitoring point	Fitted residual value/mm	Observed value/mm	Monitoring point	Fitted residual value/mm	Observed value/mm
Q01	−0.01	−9	Q31	−6.09	−77
Q02	−6.00	−18	Q32	−2.19	−62
Q03	−4.22	−20	Q33	−4.30	−54
Q04	−1.55	−22	Q34	−4.30	−45
Q05	−0.90	−27	Q35	−1.16	−34
Q06	3.84	−29	Q36	−1.90	−28
Q07	3.70	−37	Q37	1.45	−19
Q08	5.70	−44	Q38	−2.22	−18
Q09	6.81	−53	Q39	1.00	−11
Q10	6.91	−64	Q40	−0.01	−9

The curve graph after regional fitting (with edge parameters $q = 0.02994$ and $tan\beta = 0.5864$; and central region parameters $q = 0.61184$ and $tan\beta = 1.5167$) is shown in Figure 6.

TABLE 4 Table of inverted predicted parameters.

Predicted parameters	Subsidence rate q	Tangent of the influence angle $tan\beta$
Edge part or Marginal part	0.02994	0.5864
Central part or Core part	0.61184	1.5167

3. The overall distribution retains a symmetrical U-shaped characteristic, with its basic shape remaining unchanged despite variations in *tanβ*.

When adjusting expected parameters to fit the predicted curve to observation data, it remains challenging to achieve an optimal fit for both the interior and edges of the subsidence basin.

4.4 Regional inversion

Given that both the probabilistic integration method and the probability density function (PDF) method exhibit large edge fitting errors, this study proposes a regional inversion approach for the PDF method, which demonstrates a good overall fit. The objective is to reconstruct the fitting function for edge data, ensuring an accurate fit for both the edge and central regions.

For the edge data Q01-Q10 and Q31-Q40, a new fitting was performed with the fitting parameters q set to 0.02994, *tanβ* set to 0.5864, and the R-squared value at 0.988. The fitted curves from regional inversion are shown in Figure 6. The fitting residuals are shown in Table 3.

Based on the above analysis, it is recommended to adopt the probability density function (PDF) method, utilizing different predicted parameters for edge and central data. The inverted predicted parameters are presented in the following Table 4.

5 Surface subsidence trend main cross-section numerical simulation analysis comparison

5.1 Model construction

The calculations in this study were conducted using MIDAS GTS NX, a geotechnical engineering analysis software. To simulate the soil body, solid elements were employed due to their ability to accurately capture the three-dimensional stress-strain behavior of soil.

The model dimensions were set to 630 m (X) × 300 m (Y) × 351 m (Z), ensuring that boundaries were sufficiently distant from the area of interest to minimize boundary effects on simulation results. The soil material was represented using the Mohr-Coulomb model, chosen for its proven effectiveness in capturing the shear strength and failure characteristics of soil under the studied conditions. Key parameters of the Mohr-Coulomb model, including the internal friction angle (ϕ), cohesion (c), and unit weight (γ), were obtained from laboratory tests on site-collected soil samples, ensuring consistency with real-world conditions.

The boundary conditions were defined to reflect the physical constraints of the problem:

1. The upper boundary was set as a free surface, simulating an unconstrained ground surface.
2. The lower boundary constrained displacement in the Z direction, representing a rigid bedrock layer.
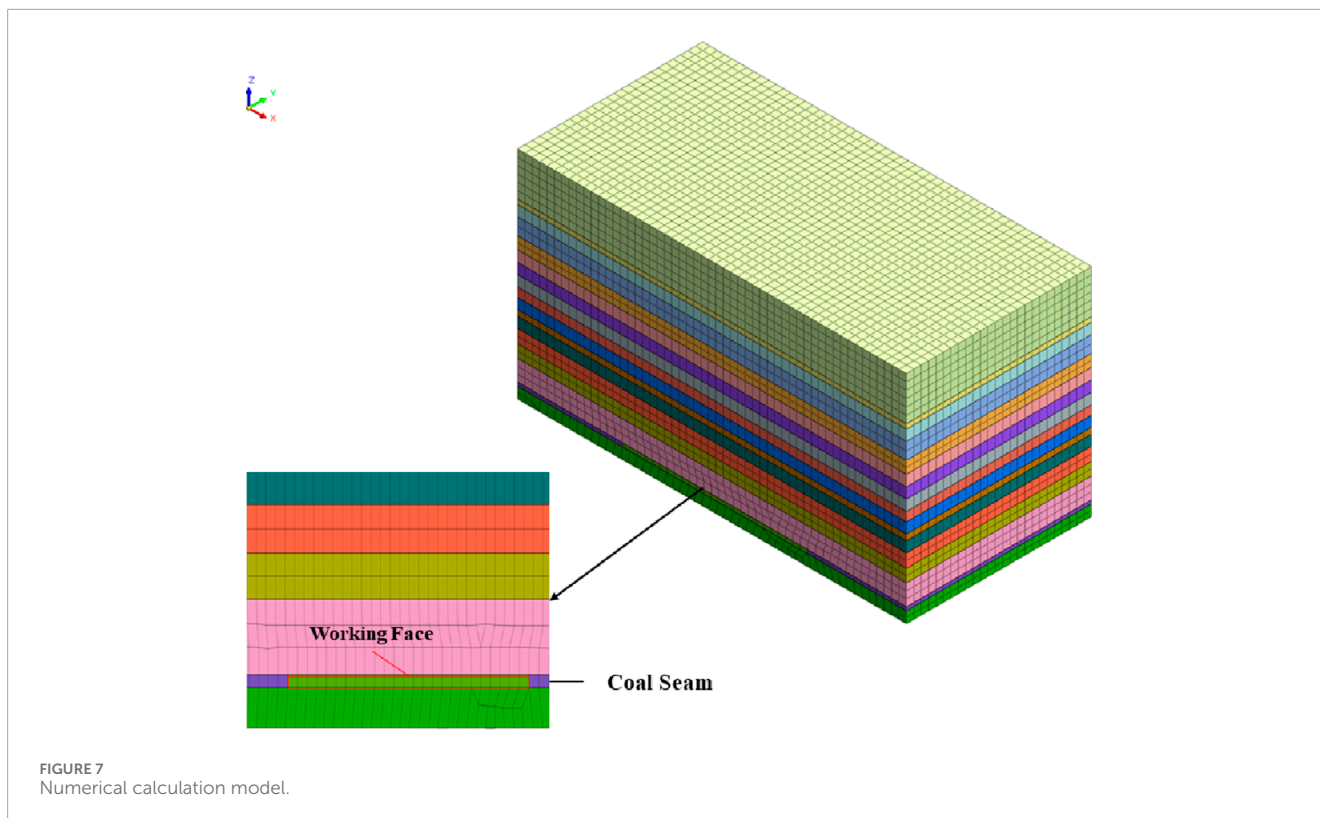
FIGURE 7
Numerical calculation model.

3. The left and right boundaries constrained displacement in the Y direction, while the front and back boundaries constrained displacement in the X direction, mimicking the semi-infinite extent of the soil in the horizontal plane.

To enhance reproducibility, the model assumes a homogeneous, isotropic soil body with no groundwater, neglecting fluid-solid coupling effects. The mesh was constructed using hexahedral solid elements with an average size of 5 m, balancing computational efficiency and accuracy.

The simulation was conducted in two stages:

1. Establishing an initial stress field under gravitational loading to reflect *in situ* conditions.
2. Applying specific loading or excavation scenarios based on the study's objectives.

The model setup is illustrated in Figure 7, providing a visual representation of the geometry and boundary conditions.

5.2 Computational results

Mining of the underground coal seam resulted in the loss of support for the overlying soil and rock mass, triggering a stress redistribution within the strata. The area adjacent to the coal pillar experienced significant pressure, leading to compressive failure of the soil and rock mass in that region (G.W. P., 2017). The simulation results are illustrated in Figure 8.

After excavation, stress redistribution induces uneven settlement within a certain range. The settlement value gradually decreases upward from the bottom of the mined-out area. On the surface, settlement decreases progressively from the center of the excavation toward both ends. The maximum surface settlement is 2.91 m.

5.3 Comparison of fitting analysis and numerical analysis

Figures 9, 10 illustrate the fitting results of the probability density function (PDF) method and the probabilistic integration method, respectively, compared with numerical calculation results. The figures clearly depict the comparison between numerical results and fitting results.

A comparative analysis of the probabilistic integration method and the PDF method reveals that the probabilistic integration method may exhibit fitting accuracy issues within specific intervals. This phenomenon likely arises from its inherent limitations in global fitting capability. In contrast, the PDF method demonstrates a high degree of consistency with numerical simulation results in overall trends. This finding suggests that the PDF method offers a significant advantage in global fitting performance.

6 Discussion

This study demonstrates that the probability density function (PDF) method outperforms the traditional probabilistic integration method (PIM) in fitting subsidence curves under insufficient mining conditions, particularly in edge regions. These results align with
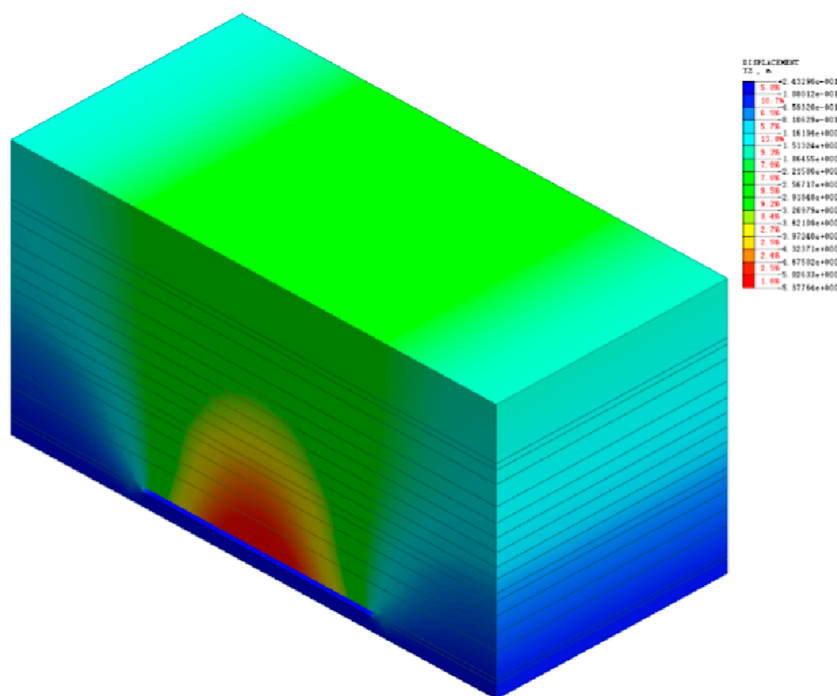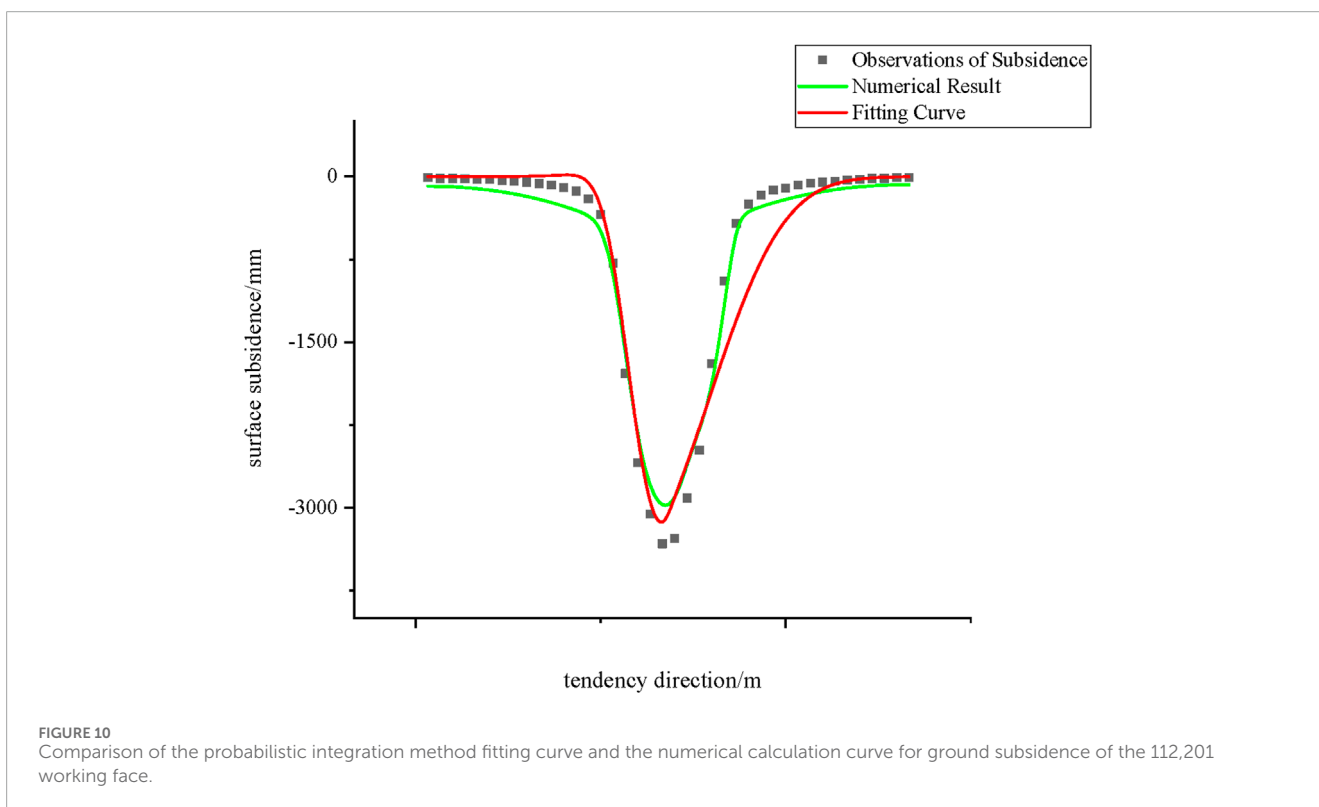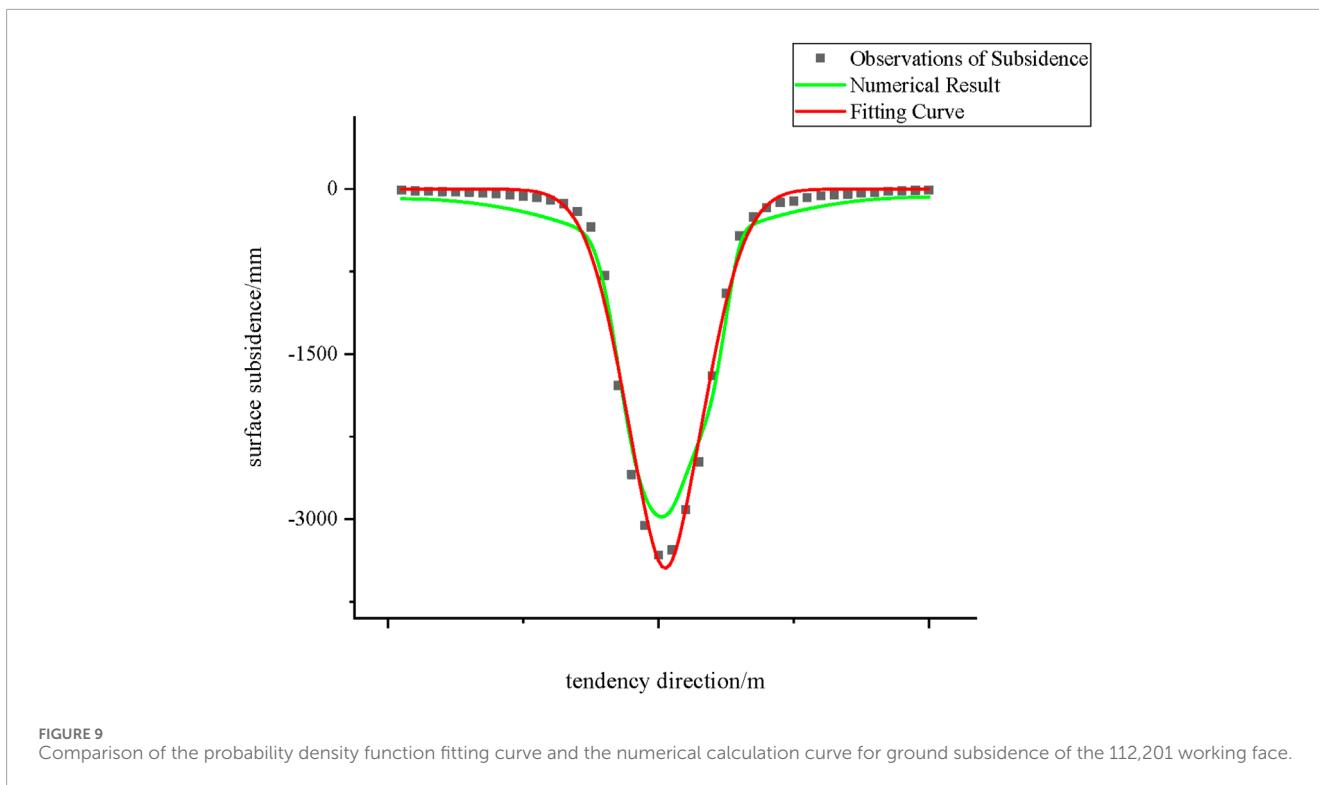
Displacement cloud diagram in the Z direction
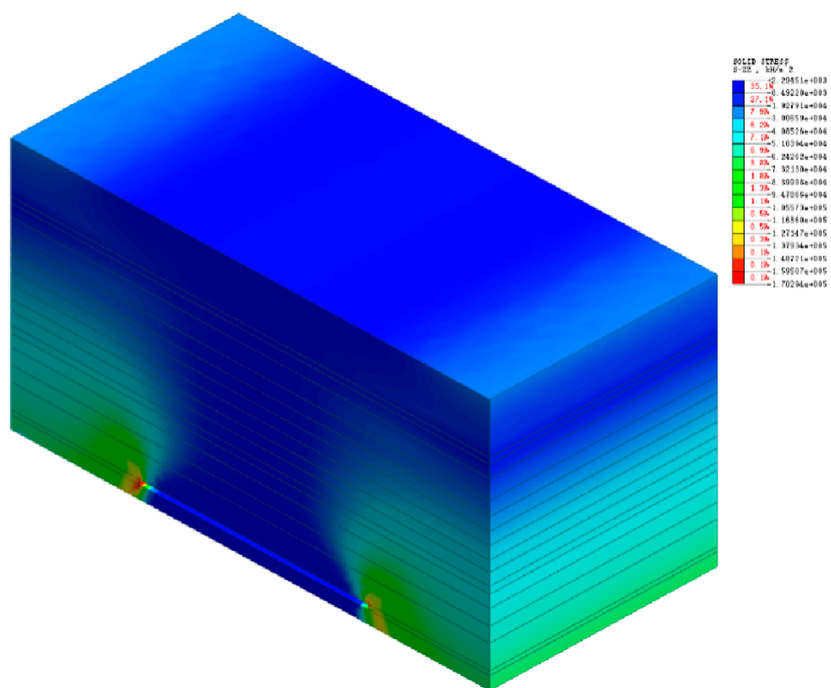
Total stress diagram in the Z direction

FIGURE 8
Displacement cloud diagram in the Z direction. Total stress diagram in the Z direction. Numerical calculation results of ground subsidence for the 112,201 working face.

FIGURE 9
Comparison of the probability density function fitting curve and the numerical calculation curve for ground subsidence of the 112,201 working face.

FIGURE 10
Comparison of the probabilistic integration method fitting curve and the numerical calculation curve for ground subsidence of the 112,201 working face.

Guo et al. (2004), who proposed the PDF method to mitigate parameter correlation issues inherent in PIM. However, our regional inversion strategy further resolves edge-fitting discrepancies, a limitation noted in studies by Han (2021) and Zhao et al. (2022).

Compared to recent advancements like the segmented correction model by Tao et al. (2023) for thick loose layers or the hybrid machine-learning approach by Chi et al. (2023), our method simplifies parameterization by eliminating the need for additional

coefficients (e.g., mining coefficient C), enhancing practicality for field applications. While Hu et al. (2023) integrated InSAR and genetic algorithms to improve PIM, our focus on sub-region fitting offers a computationally efficient alternative without requiring extensive remote sensing data.

A key strength of this work is its adaptability to asymmetric subsidence basins, a challenge poorly addressed by classical PIM (Liu and Dai, 2016). However, limitations persist: The model assumes homogeneous strata, whereas complex geological conditions (e.g., reverse faults or backfill mining) may necessitate further modifications, as explored by Luo et al. (2024) and Huo et al. (2023). The reliance on localized observation data limits generalizability across diverse mining geometries.

These findings contribute to the broader discourse on subsidence prediction by validating the PDF method's robustness under insufficient mining and proposing a hybrid fitting framework. Future work should explore integrating regional inversion with time-dependent models (e.g., Zhang et al., 2020) to address dynamic subsidence.

7 Conclusion

(1) The subsidence curves of the study area were fitted using both the probabilistic integration method and the probability density function (PDF) method. Analysis results indicate that the PDF method provides a superior fit. The probabilistic integration method exhibits several drawbacks, including strong correlation between predicted parameters, rapid convergence, and relatively large errors in edge data during the fitting process.

(2) To address the issue of poor edge fitting, a regional fitting approach was adopted, resulting in a closer match to surface deformation and improved fitting accuracy. This method enhances the precision of predicted surface deformation and demonstrates practical applicability.

(3) A comparison of the fitting performance of the PDF method and the probabilistic integration method against numerical simulation results shows that the PDF method exhibits a higher degree of consistency with the overall trend of numerical simulations.

Data availability statement

The original contributions presented in the study are included in the article/supplementary material, further inquiries can be directed to the corresponding author.

References

Ahmadi, M., Torkashvand, A., Badraddini, A., Sarfarazi, V., and Jahanmiri, S. (2023). Investigation of the influence of tunneling on bridge foundation in urban area. *Geotechnical Geol. Eng.* 41 (4), 2481–2499. doi:10.1007/s10706-023-02410-y

Bing, H., Yan, Z., Qiang, F., and Hou, H. (2021). Study on mining subsidence of mineral deposit and overburden stability based on probability density function. *IOP Conf. Ser. Earth Environ. Sci.* 781, 022078. doi:10.1088/1755-1315/781/2/022078

Author contributions

WD: Conceptualization, Investigation, Writing – original draft. MG: Methodology, Validation, Writing – original draft. JL: Methodology, Resources, Writing – review and editing. YZ: Formal Analysis, Supervision, Writing – review and editing. YM: Data curation, Writing – review and editing. HD: Data curation, Validation, Visualization, Writing – review and editing. BJ: Conceptualization, Formal Analysis, Resources, Writing – review and editing. LF: Data curation, Resources, Writing – review and editing. ZL: Formal Analysis, Resources, Supervision, Writing – review and editing.

Funding

Conflict of interest

Author WD was employed by Shanxi Xiaobaodang Mining Co.,Ltd. Authors MG, JL, and YZ were employed by Shanxi Coalbed Methane Development Co.,Ltd. Author ZL was employed by Hebei Civil Engineering Co., Ltd.

The remaining authors declare that the research was conducted in the absence of any commercial or financial relationships that could be construed as a potential conflict of interest.

Generative AI statement

The author(s) declare that no Generative AI was used in the creation of this manuscript.

Publisher's note

Cai, Y., Jin, Y., Wang, Z., Chen, T., Wang, Y., Kong, W., et al. (2023). A review of monitoring, calculation, and simulation methods for ground subsidence induced by coal mining. *Int. J. coal Sci. & Technol.* 10 (1), 32. doi:10.1007/s40789-023-00595-4

Chen, S., Lei, W., Yang, X., Fang, X., and Jiang, C. (2021). Research on prediction model of mining subsidence in thick unconsolidated layer mining area. *IEEE Access* 9, 23996–24010. doi:10.1109/access.2021.3056873

Chi, S., Wang, L., and Yu, X. (2023). A new method for calculating prediction parameters of surface deformation in the mining area. *Appl. Sci.* 13 (14), 8030. doi:10.3390/app13148030

Grant, A. (2017). *Originals: how non-conformists move the world.* Penguin.

Guo, Q., Chen, H., Luo, J., Wang, X., Wang, L., Lv, X., et al. (2022). Parameter inversion of probability integral method based on improved crow search algorithm. *Arabian J. Geosciences* 15 (2), 180. doi:10.1007/s12517-022-09457-w

Guo, W., Liu, D., and Bai, E. (2004). Correction of the subsidence curve formula based on the probability integration method. *J. Henan Polytech. Univ. Nat. Sci. Ed.* 35 (3), 357–362. doi:10.13225/j.cnki.jccs.2004.02.007

G.W. P. (2017). *Design analysis in rock mechanics.* 3rd ed. London: Taylor & Francis. doi:10.1201/9780203968253

Han, Y. (2021). Research on the acquisition and application of predicted parameters of the probability integration method. *Mine Surv.* 49 (4), 15–19. doi:10.3969/j.issn.1001-358X.2021.04.004

Hu, L., Jie, Z., Lian, X., Zhao, X., Lei, X., and Gong, X. (2023). Inversion of subsidence parameters and prediction of surface dynamics under insufficient mining. *J. Min. Sci.* 59 (4), 693–704. doi:10.1134/s106273912304021x

Huo, W., Li, H., Guo, G., Wang, Y., and Yuan, Y. (2023). Surface subsidence prediction method for backfill mining in shallow coal seams with hard roofs for building protection. *Sustainability* 15 (22), 15791. doi:10.3390/su152215791

Jiang, T., Zhu, C., Qiao, Y., Sasaoka, T., Shimada, H., Hamanaka, A., et al. (2024). Deterioration evolution mechanism and damage constitutive model improvement of sandstone–coal composite samples under the effect of repeated immersion. *Phys. Fluids* 36 (5). doi:10.1063/5.0208619

Li, J., Yu, X., and Liang, Y. (2020). A prediction model of mining subsidence in thick loose layer based on probability integral model. *Earth Sci. Res. J.* 24 (3), 367–372. doi:10.15446/esrj.v24n3.90111

Li, P., Li, Y., Li, Q., Cao, Z., and Wang, L. (2022). A novel analytical model of mining subsidence considering time effect based on the probability integral theory. *Sustainability* 14 (21), 14443. doi:10.3390/su142114443

Liu, B., and Dai, H. (2016). Research development and origin of probability integral method. *J. Min. Strata Control Eng.* 21 (2), 1–3. doi:10.13532/j.cnki.cn11-3677/td.2016.02.001

Lou, J. (2024). A parameter inversion method for the probability integral method based on robust ridge estimation. *Front. Earth Sci.* 11, 1330163. doi:10.3389/feart.2023.1330163

Luo, J., Li, Y., Guo, Q., Meng, X., and Wang, L. (2024). Research on the surface subsidence characteristics and prediction models caused by coal mining under the reverse fault. *Sci. Rep.* 14 (1), 25316. doi:10.1038/s41598-024-75182-x

Shi, M., Yang, H., Wang, B., Peng, J., Gao, Z., and Zhang, B. (2021). Improving boundary constraint of probability integral method in SBAS-InSAR for deformation monitoring in mining areas. *Remote Sens.* 13 (8), 1497. doi:10.3390/rs13081497

Tao, W., Guangli, G., Huaizhan, L., Wang, L., Jiang, Q., and Jiang, C. (2023). A novel probability integral method segmental modified model for subsidence prediction applicable to thick loose layer mining areas. *Environ. Sci. Pollut. Res. Int.* 30 (18), 52049–52061. doi:10.1007/s11356-023-26021-5

Wang, J., Yang, & others, Wei, X., Shi, X., and Yao, S. (2021). Prediction of longwall progressive subsidence basin using the Gompertz time function. *Rock Mech. Rock Eng.* 55, 379–398. doi:10.1007/s00603-021-02664-z

Wang, Z., Zhao, Y., Wang, P., Wang, X., Jiang, A., Zhang, G., et al. (2024). Refined subsidence monitoring and dynamic prediction in narrow and long mining areas based on InSAR and probabilistic integral method. *Sci. Rep.* 14 (1), 28009. doi:10.1038/s41598-024-76037-1

Wei, T., Guo, G., Li, H., Wang, L., Jiang, Q., and Jiang, C. (2023). A novel probability integral method segmental modified model for subsidence prediction applicable to thick loose layer mining areas. *Environ. Sci. Pollut. Res.* 30 (18), 52049–52061. doi:10.1007/s11356-023-26021-5

Xuemin, X., Yikai, Z., Zhihui, Y., Xiao, L., Liu, X., Chen, L., et al. (2021). Predicting mining-induced dynamic deformations for drilling solution rock salt mine based on probability integral method and Weibull temporal function. *Int. J. Remote Sens.* 42 (2), 639–671. doi:10.1080/01431161.2020.1813345

Yan, W., Chen, J., and Yan, Y. (2019). A new model for predicting surface mining subsidence: the improved lognormal function model. *Geosciences J.* 23 (1), 165–174. doi:10.1007/s12303-018-0008-1

Yuan, Y., Li, H., Zhang, H., Zhang, Y., and Zhang, X. (2020). Improving reliability of prediction results of mine surface subsidence of Northern Pei County for reusing land resources. *Appl. Sci.* 10 (23), 8385. doi:10.3390/app10238385

Zhang, J., Zhang, P., and Ji, X. (2024). Prediction of surface subsidence in Gequan coal mine based on probability integral and numerical simulation. *Acad. J. Eng. Technol. Sci.* doi:10.25236/AJETS.2024.070102

Zhang, L., Cheng, H., Yao, Z., and Wang, X. (2020). Application of the improved Knothe time function model in the prediction of ground mining subsidence: a case study from Heze City, Shandong Province, China. *Appl. Sci.* 10 (9), 3147. doi:10.3390/app10093147

Zhao, B., Guo, Y., Mao, X., Zhai, D., Zhu, D., Huo, Y., et al. (2022). Prediction method for surface subsidence of coal seam mining in loess donga based on the probability integration model. *Energies* 15 (6), 2282. doi:10.3390/en15062282

Zi-Tong, Z., He-Qing, M., and Ka-Veng, Y. (2024). Probability density function modelling and credible region construction for multivariate, asymmetric, and multimodal distributions of geotechnical data. *Struct. Saf.* 107, 102429. doi:10.1016/j.strusafe.2023.102429